Available online at www.sciencedirect.com

ScienceDirect

Procedia Structural Integrity 3 (2017) 18–24

Structural Integrity Procedia

www.elsevier.com/locate/procedia

XXIV Italian Group of Fracture Conference, 1-3 March 2017, Urbino, Italy

Fracture toughness of highly deformable polymeric materials

Roberto Brighenti[a]*, Andrea Carpinteri[a], Federico Artoni[a]

[a]*Dept. of Engineering & Architecture – University of Parma, Parco Area delle Scienze 181/A, 43124 Parma, Italy*

Abstract

A fundamental requirement for safety design of structural components is flaw tolerance. In this field, the soft materials have a unique ability to bear external loads despite the presence of defects, due to their pronounced deformability. Unlike traditional materials, which have an enthalpic elasticity, the mechanical response of a polymer-based material is governed by the state of internal entropy of a molecular network which has a great ability to rearrange the material structure and shape so to minimize the local detrimental effect of flaws. For a correct estimation of the fracture toughness of these materials, a proper knowledge of this entropic effect is needed. In the present research, the mechanical behaviour up to failure of silicone-based cracked plates is examined by taking into account the time-dependent effects. Experimental and theoretical aspects are discussed in order to understand the defect tolerance of such materials.

Keywords: Fracture Mechanics; Polymer network; Fracture toughness; Damage tolerance

1. Introduction

Fracture toughness is an important property to be taken into account for defect tolerance-based design of structural components. Such a property quantifies the ability of a material to reduce the effect of flaws on the global strength of the structures. In this paper, we present the results of some experimental tests performed on flawed specimens made by a common silicone-based polymer. This material has a particular stress-strain curve, which is nearly hyperelastic up to failure, with a negligible effect of plasticity or internal damage until the final brittle failure occurs (Brighenti 2016).

* Corresponding author. Tel.: +39 0521 905910; fax: +39 0521 905924.
E-mail address: brigh@unipr.it

10.1016/j.prostr.2017.04.004

Nomenclature

$2a$	Initial crack length
$c(a)$	Decreasing function of a that reduces the actual applied remote stress during crack growth
E,ν	Young modulus and Poisson's ratio of the material, respectively
G	Energy release rate
K_I	Stress-Intensity Factor (SIF) in Mode I
K_I^*	Dimensionless Stress-Intensity Factor in Mode I
L_{cr}	Final crack length, measured along the crack path, after the final failure
t	Thickness of the specimen
W	Plate width
$\alpha = 2a/W$	Dimensionless crack length
γ	Fracture energy per unit cracked surface
$\dot{\varepsilon}$	Strain rate
η	Average radius of the micro voids existing in the material
λ	Stretch ratio
λ_S	Surface stretch
Ψ,Ψ_{el}	Total deformation energy and elastic energy, respectively
$\boldsymbol{\sigma},\sigma_{ij}$	Cauchy stress tensor
σ_∞	Remote applied stress

The mechanical behaviour of a polymeric material is quite different from that of a crystalline material (Doi 2013). As a matter of fact, in the absence of external forces, the microstructure of a crystal is in a stable equilibrium state that minimizes the energy of the system. The external forces produce displacements of the molecules and lead to a new equilibrium state with an increment of internal energy equal to the external work (in absence of non-conservative forces). This behaviour is called "enthalpic elasticity" because it's governed by internal energy. A polymer has a microstructure which is not made of crystalline units, but is characterized by a network of long molecular chains entangled all together. In absence of external forces, each chain is in a thermodynamical equilibrium state, i.e. the effective shape of the chain is one of the infinite possible configurations that the material can have for the current energy level.

The absolute temperature and the end-to-end distance of a chain defines its internal energy, while the energy of the unit volume of the material is obtained by adding up the energy of a single chain weighted by the probability density function of the chains' end-to-end distance distribution. It is clear why this kind of behaviour is called "entropic elasticity": the configuration of a chain is known only in probabilistic term, and it is ruled by the order of the system. Physically, the effect of external forces is to stretch the macromolecule in the direction of the applied load; mathematically, the external forces "stretch" the density probability function and the states with longer chains aligned in the load direction become more probable than before the deformation (Treloar 1973).

In the vicinity of a defect like a crack or a notch, the stress level abruptly increases within a narrow region close to the crack tip or notch root, and the chains are very stretched in the traction direction. Moreover if the external load slowly increases in time, the polymeric chains have the possibility to rearrange and change their shape without varying the global energy (Flory 1989). In fact, the part of the polymeric network close to the crack tip is in a much more ordered state with respect the other regions far from the crack because of the chains alignment. For a polymer network, fracture mechanics is ruled by non-local phenomena, and the conventional intensification of stress loses importance. Further, fracture toughness greatly depends on the strain rate because of the time-dependent phenomena occurring at the nanoscale level.

In the present paper, the fracture toughness is measured from some experimental tests made on polymer-based cracked plates. The values obtained are related to the strain rate and to the geometry of the specimen. Moreover, the evaluation of the fracture energy allows us to determine the intrinsic defect size through the use of the cavitation criterion to assess failure.

2. Crack growth modeling in highly deformable materials

Failure of the polymer networks can be interpreted by applying a model known as cavitation criterion (Fond 2001). Following this criterion, intrinsic micro-spherical voids – subjected to an internal hydrostatic pressure in equilibrium with the stress field – are assumed to exist embedded in the material. When the internal pressure grows up to a critical value, the equilibrium is not possible and, therefore the inflation of the voids became instable, leading to a brittle failure. The growth process of the cavity usually shows a stiffening behaviour due to the unfolding of the long molecular chains surrounding the void (Lev 2016). According to other authors, the polymer's failure is ruled by the so-called fibril creep mechanism (Jie 1998).

For sufficiently high strain rates, the elastomeric materials show, with a good approximation, an elastic behaviour and, therefore, the Griffith's energy balance for a penny-shaped circular crack of radius η can be written as follows:

$$\frac{\partial\left(W_F+\Psi+G\right)}{\partial\eta}<0 \tag{1}$$

where W_F is the potential energy of the external forces, Ψ is the deformation energy stored in the material, and $G=4\pi\eta^2\gamma$ is the fracture energy (energy per unit surface γ). If the external loads are statically applied and the fracture failure develops instantaneously, W_F is negligible and the above balance becomes:

$$\frac{\partial\Psi}{\partial\eta}>4\pi\eta^2\gamma \tag{2}$$

in which the reduction of internal energy during the fracture propagation is taken into account.

For an infinite new-Hookean medium with a spherical void having an initial radius η, the critical value of the hydrostatic pressure can be related to the fracture energy release rate G:

$$G=\frac{\partial\Psi}{\partial\eta}=\lim_{\eta\to0}\frac{\Psi\left(\eta+d\eta\right)-\Psi\left(\eta\right)}{2\pi\eta d\eta} \tag{3}$$

where the energy is evaluated for a penny-shaped crack with radius that increases from η to $\eta+d\eta$.

The term $\Psi\left(\eta\right)$ can be evaluated from the solution of the elastic problem of a spherical void in an infinite medium subjected to an internal pressure p; the use of the above mentioned elastic solution (Jie 1998) in (3) leads to:

$$G=2E\eta\frac{1+\lambda_S^2-2\lambda_S^{-1}}{3} \tag{4}$$

where E is the Young modulus of the material and λ_S is the surface stretch, which can be also related to the pressure p acting inside the spherical void through the relation $p\left(\lambda_S\right)=\left(5-4\lambda_S^{-1}-\lambda_S^{-4}\right)E/6$, with $\lambda_S=S'/S=1+2d\eta\cdot\eta^{-1}$. Note that S,S' are the external surfaces of the initial and final spherical void, respectively (Lin 2004). By substituting $p\left(\lambda_S\right)$ in Eq. (4), with the restriction $p>\left(11/18\right)E$, the failure criterion can be formulated under the hypothesis that the energy release rate G is equal to the fracture energy of the material γ, while the pressure p acting inside the void is equal to the hydrostatic stress in the material $p=\sigma_{ii}/3$ (the repeated index stands for summation over such an index, i.e. $\sigma_{ii}=\sum_{j=1}^{3}\sigma_{jj}$). The failure condition is fulfilled when the following inequality holds:

$$\frac{2E\eta}{3}\cdot\left[\frac{16}{25\left(1-\frac{2\sigma_{ii}}{5E}\right)^2}-\frac{3}{2}+\frac{\sigma_{ii}}{E}\right]-\gamma\geq 0 \tag{5}$$

Note that (5) requires the knowledge of the average radius η of the voids which are initially present in the material.

As soon as the critical condition for void expansion is attained, it can be assumed that the stress state in that point vanishes because of the material failure occurring in the small region around such a point of cavitation.

3. Experimental tests

In order to quantify the mechanical response and the fracture toughness of flawed elastomeric structural components under tension up to the final failure, different pre-cracked thin plates are herein examined. The sheets are made of a common silicone polymer obtained from the cross-linking of two vinyl-terminated polydimethylsiloxane matrix and an hydride terminated siloxane curing agent, with a Pd-catalyzed hydrosilylation, also commercially known as Sylgard®. The specimens are tested under simple monotonic tension at different strain rates. Then, experimental results are elaborated with Digital Image Correlation (DIC) technique to obtain the deformation field in the samples during the tests.

The sheets have an initial elastic modulus equal to about $E=0.98\,MPa$ and Poisson's ratio $\nu\cong 0.42$. All the main geometric characteristics of the tested specimens are shown in Table 1. Four values of the initial crack length are examined and, for each length, three tests are made with different values of strain rate (Tab. 1).

In Fig. 1 a group of specimens (with an initial crack equal to 50 mm) during the traction test are shown. By comparing the images it is clearly visible the characteristic evolution of the crack's shape. The crack tip is subjected to a remarkable blunting, and the regions along the crack are transversely compressed and show out-of-plane displacements. Therefore, two different crack tips appear on both sides of the initial crack's branches, developing in the direction of the applied load. The observed failure mechanism is brittle and leads to an instantaneous rupture of the material. In Fig. 2, some images of the specimens with the highlighted crack paths developed at the end of the test, are reported.

In Fig. 3 and Fig. 4 some representative maps of the Green-Lagrange large strain obtained from digital image correlation are displayed (see Blaber 2015 for an explanation of the algorithm adopted).

Table 1. Characteristics and geometry of the specimens. The applied strain rates are equal to $\dot{\varepsilon}_{y1}=5.769\cdot 10^{-3}s^{-1}$, $\dot{\varepsilon}_{y2}=9.615\cdot 10^{-4}s^{-1}$, $\dot{\varepsilon}_{y3}=1.603\cdot 10^{-4}s^{-1}$.

Spec. No.	W (mm)	$2a$ (mm)	t (mm)	$2a/W$ (---)	$\dot{\varepsilon}_y$ (s^{-1})
C2a	112	20	2.75	0.179	$\dot{\varepsilon}_{y1}$
C2b	112	20	2.85	0.179	$\dot{\varepsilon}_{y2}$
C2c	112	20	2.75	0.179	$\dot{\varepsilon}_{y3}$
C3a	112	30	3.00	0.268	$\dot{\varepsilon}_{y1}$
C3b	112	30	3.00	0.268	$\dot{\varepsilon}_{y2}$
C3c	112	30	2.60	0.268	$\dot{\varepsilon}_{y3}$
C4a	112	40	2.75	0.357	$\dot{\varepsilon}_{y1}$
C4b	112	40	1.80	0.357	$\dot{\varepsilon}_{y2}$
C4c	112	40	2.00	0.357	$\dot{\varepsilon}_{y3}$
C5a	112	50	2.85	0.446	$\dot{\varepsilon}_{y1}$
C5b	112	50	2.95	0.446	$\dot{\varepsilon}_{y2}$
C5c	112	50	3.05	0.446	$\dot{\varepsilon}_{y3}$

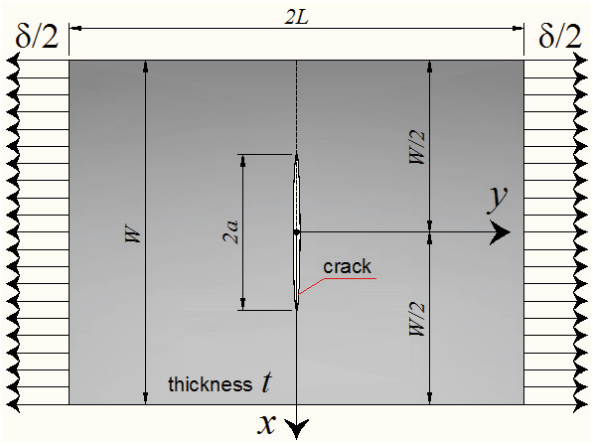

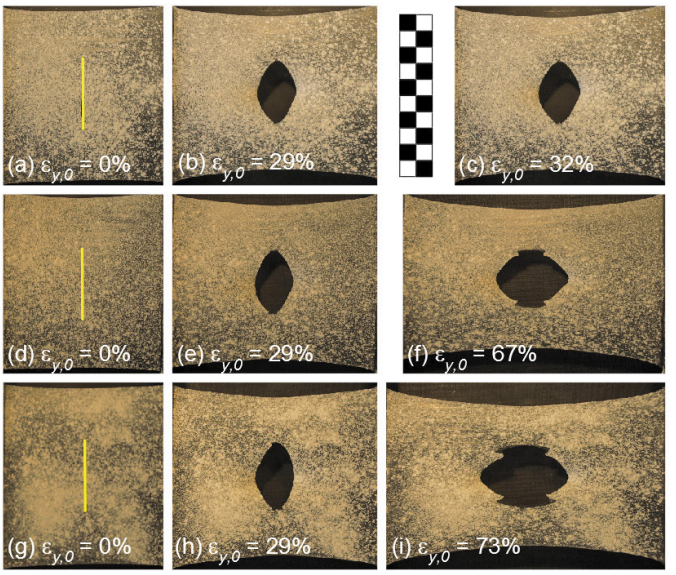

Fig. 1. Images of the specimens with the initial crack equal to 50 mm in the initial (a, d, g), intermediate (b, e, h) and final configuration at incipient failure (c, f, i). The strain rate is $\dot{\varepsilon}_{y1} = 5.769 \cdot 10^{-3} s^{-1}$ (1st row), $\dot{\varepsilon}_{y2} = 9.615 \cdot 10^{-4} s^{-1}$ (2nd row), $\dot{\varepsilon}_{y3} = 1.603 \cdot 10^{-4} s^{-1}$ (3rd row).

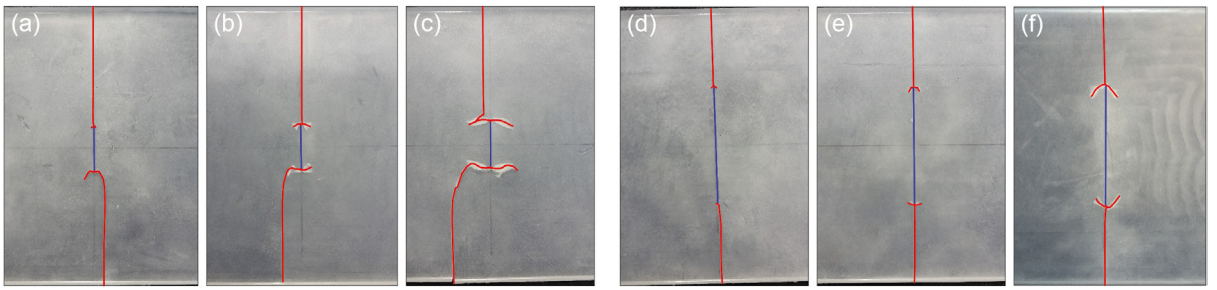

Fig. 2. Images of some specimens after the test: strain rate $\dot{\varepsilon}_{y1} = 5.769 \cdot 10^{-3} s^{-1}$ (a, d), strain rate $\dot{\varepsilon}_{y2} = 9.615 \cdot 10^{-4} s^{-1}$ (b, e), strain rate $\dot{\varepsilon}_{y3} = 1.603 \cdot 10^{-4} s^{-1}$ (c, f). Specimens with 50 mm crack (a, b, c); specimens with 20 mm crack (d, e, f).

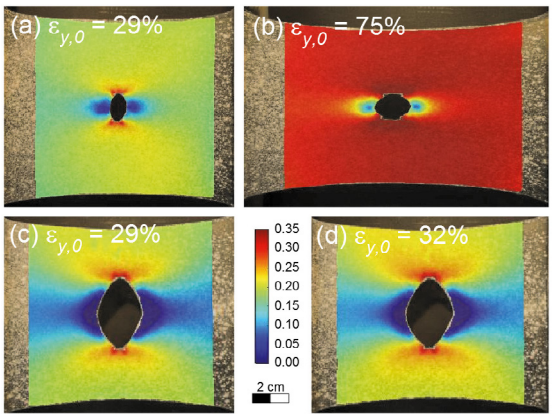

Fig. 3. Eyy strain maps for the tests at $\dot{\varepsilon}_{y1} = 5.769 \cdot 10^{-3} s^{-1}$: specimens with 20 mm crack at intermediate and final state (a, b), specimens with 50 mm crack at initial and final state (c, d).

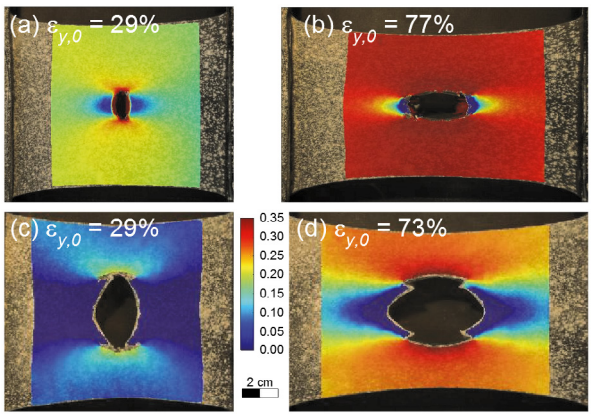

Fig. 4. Eyy strain maps for the tests at $\dot{\varepsilon}_{y3} = 1.603 \cdot 10^{-4} s^{-1}$: specimens with 20 mm crack at intermediate and final state (a, b), specimens with 50 mm crack at initial and final state (c, d).

4. Fracture energy estimation

The fracture toughness of the material is related to the energy per unit area necessary to produce failure, i.e.

$$\gamma = (\Psi - \Psi_{el}) / (L_{cr} \cdot t) \tag{6}$$

where Ψ is the total energy stored in the specimen at incipient failure and Ψ_{el} is the elastic energy restored after the final fracture collapse, while L_{cr} is the length of the whole developed crack. In Fig. 5a, the fracture energy evaluated according to (6) is shown for all the tested specimens in the simplest case $\Psi_{el} = 0$, i.e. no elastic energy is assumed to be recovered in the material upon unloading, while Ψ is evaluated by integrating the experimental force-displacement curve.

The fracture energy appears to be significantly lower for high strain rates (see dashed line in the figure that refers to the highest strain rate) . The fracture energy can be computed from the stress intensity factor (SIF) in Mode I, K_I, for a straight crack of initial length $2a$ and final length W :

$$\Psi - \Psi_{el} = 2t \cdot \int_a^{W/2} \frac{\left(c(a) \cdot \sigma_\infty \sqrt{\pi a} \cdot K_I^*\right)^2}{E} da \tag{7}$$

$c(a)$ being a reduction factor accounting for the decrease of the remote applied stress during the crack propagation (Nobile et al. 2002).

For an infinite strip of width W containing a transversal crack with initial length $2a$ and subjected to a remote opening stress σ_∞, the dimensionless SIF is given by (Murakami 1986):

$$K_I^* = \left(1 - 0.025\alpha^2 + 0.06\alpha^4\right) \cos^{-1/2}\left(\frac{\pi}{2}\alpha\right) \tag{8}$$

where $\alpha = 2a/W$ is the dimensionless crack length. By replacing the above SIF expression in (7), and assuming $\sigma_{\infty,u} = F_u / (t \cdot W)$, F_u being the ultimate tensile force at incipient failure, the fracture energy becomes:

$$\gamma = \frac{\Psi - \Psi_{el}}{L_{cr} \cdot t} = \frac{\pi \cdot \sigma_{\infty,u}^2 W^2}{2EL_{cr}} \int_\alpha^1 \alpha \cdot c^2(\alpha) \cdot \frac{\left(1 - 0.025\alpha^2 + 0.06\alpha^4\right)^2}{\cos\left(\frac{\pi}{2}\alpha\right)} d\alpha \tag{9}$$

By adopting for $c(a)$ a polynomial decreasing function of the crack length a, the fracture energy γ can be evaluated once the experimentally measured ultimate stresses $\sigma_{\infty,u}$ is known; the resulting values are reported in Fig. 5b.

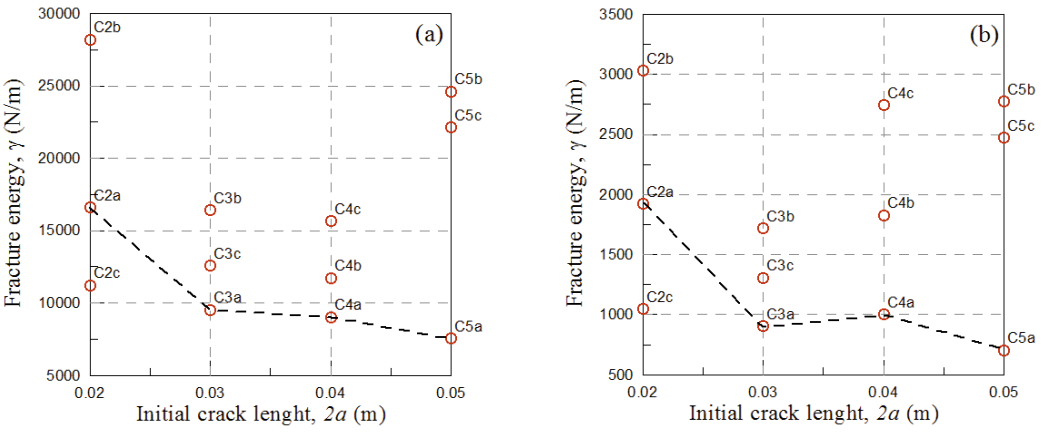

Fig. 5.Fracture energy calculated using Eq. (6) vs initial crack length for the different strain rates (a). Fracture energy calculated using Eq. (7) vs initial crack length for the different strain rates (b).

By comparing the calculated fracture energy according to (9) (Fig. 5b) with those in Fig. 5a, it can be noticed that the elastic contribution Ψ_{el} is relevant and cannot be neglected; in fact from the observation of Fig. 2 the specimens after failure do not show any damage but in the narrow fracture lines developed from the initial crack. The fracture energy has been found to be equal to about $\gamma \cong 1\ kN/m$ for the highest strain rates.

Finally, by assuming the existence of a uniform stress distribution in the ligaments of the specimen because of the strong crack blunting occurring in the cracked sheet, i.e. $\sigma_{22} = \sigma_y \cong F_u / \left(t \cdot \left(W - 2a\right)\right)$, ($\sigma_{11} = \sigma_{33} = 0$); by using Eq. (5) the average radius η of the voids initially present in the material can be estimated. In Fig. 6 the obtained values of η are reported vs the initial crack length for the different strain rates. Neglecting some dispersed results, it can be observed that the size of the intrinsic initial micro voids is equal to about $\eta \cong 0.2\text{-}0.4$ mm.

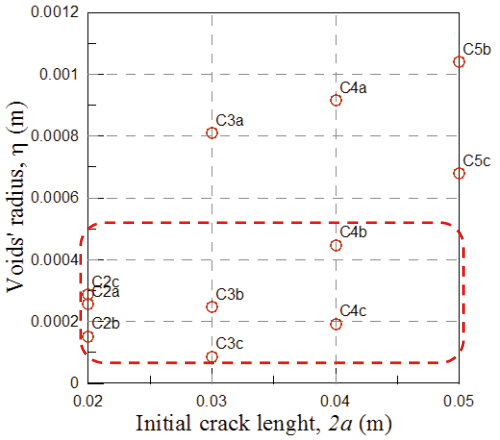

Fig. 6. Average radius of the voids vs. initial crack length for the different strain rates.

Conclusions

In the present paper, the damage tolerance estimated in term of the fracture toughness in highly-deformable polymeric materials has been examined. The results of experimental tests conducted on pre-cracked tensile elastomeric silicone specimens have been presented in relation to the applied strain rate and the initial crack length. The fracture energy has been finally determined and by using a cavitation-based failure criterion suitable for polymers, the size of the microdefects present in the material has been estimated.

On the basis of the high fracture energy values determined in the present study, a strong defect tolerance can be recognized for the highly deformable silicone polymer.

References

Blaber, J., Adair, B., Antoniou, A., 2015. Ncorr: open-source 2D image correlation Matlab software, Experim. Mech. 55, 1105–1122.

Brighenti, R., Carpinteri, A., Artoni, F., 2016. Defect sensitivity to failure of highly deformable polymeric materials, Theor. Appl. Fract. Mech. (doi: 10.1016/j.tafmec.2016.12.005)

Doi, M., 2013. Soft Matter Physics, Oxford Univ. Press, UK.

Flory, P.J., 1989. Statistical Mechanics of Chain Molecules, Hansen-Gardner, Cincinnati, Ohio.

Fond, C., 2001. Cavitation criterion for rubber materials: a review of void-growth models, J. Pol. Sci.: Part B: Polym. Phys 39, 2081–2096.

Jie, M., Tang, C.Y., Li, Y.P., Li, C.C., 1998. Damage evolution and energy dissipation of polymers with crazes, Theor. Appl. Fract. Mech. 28 (3) 165–174.

Lev, Y., Volokh, K.Y., 2016. On cavitation in rubberlike materials, J. App. Mech. 83 (4), 0044501-1-0044501-4.

Lin, Y.Y., Hui, C.Y., 2004. Cavity growth from crack-like defects in soft materials, J. Fract. 126, 205-221

Murakami, Y. (ed.), 1987. Stress Intensity Factors Handbook, Pergamon press.

Nobile, L., Ricci P., Viola, E., 2002. In modelling the dynamic behaviour of cracked plane structures, Convegno IGF XVI, Catania 2002.

Treloar, L.R.G., 1973. The elasticity and related properties of rubbers, Rep. Prog. Phys. 36, 755–826.